

# Lab 3:PMT Energy Measurements

Diego McDonald(primary), Lily, Dan

Experiment Date: Oct 26, 2017; Submission Date: Nov 13, 2017

## 1 Statement of Purpose

The purpose of this lab is to learn about making pulse-height measurements, as well as taking pulse height spectra to measure the energy of gamma ray sources. In doing so, we will also study the relationship between high-voltage bias and the output of a photomultiplier tube (PMT), as well as the difference between a sodium-iodide scintillator detector and a plastic scintillator detector.

## 2 Theory

### 2.1 Radioactive Decays

The sources in this lab all undergo different decay processes. We use a few different radioactive sources including Cs-137, Ba-133, Na-22, and Co-60:

#### 2.1.1 Cesium-137



Cesium-137, with a half-life of  $\sim 30$  years, decays through the above process ( $\beta^-$ ) with a  $\sim 95\%$  probability. The alternative can be viewed in the decay scheme below:

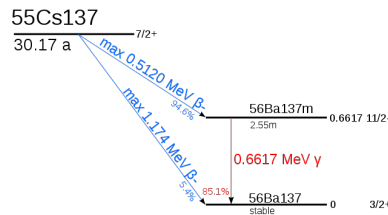


Figure 1: Decay scheme for Cs-137. [1]

As made apparent in the decay scheme above, the most probable decay process includes to a  $\beta^-$  decay to a meta-stable state of Ba-137, and a secondary decay to a stable state of Ba-137 through the emission of a photon,  $\gamma$ , of energy 0.6617 MeV, shown in Equation 1. This is the physical phenomena responsible for the signals generated using a Cs-137 source.

### 2.1.2 Barium-133



Barium-133, with a half-life of  $\sim 10$  years, decays through electron capture to an excited state of Cesium-133, which in turn decays into a stable state, releasing two photons of energies 437KeV and 383KeV, respectively. This decay scheme can be viewed below:

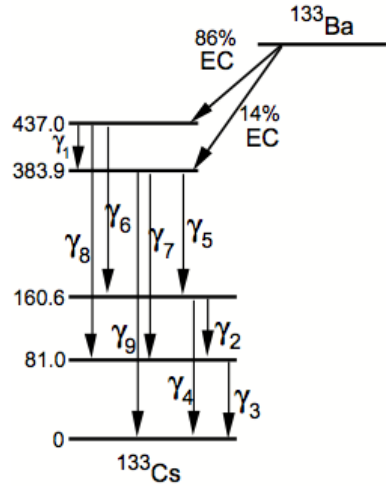


Figure 2: Decay Scheme for Ba-133. [2]

### 2.1.3 Cobalt-60



Cobalt-60, with a half-life of  $\sim 5.3$  years, decays through the  $\beta^-$  process shown above, emitting two photons with energies 1.17MeV and 1.33MeV. The other possible decay processes can be viewed below:

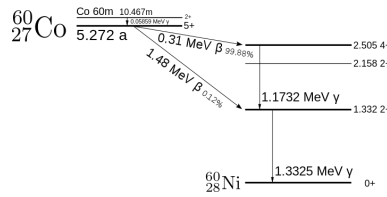
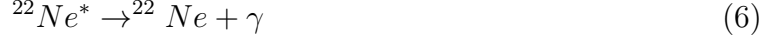


Figure 3: Decay Scheme for Co-60. [1]

### 2.1.4 Sodium-22



Sodium-22, with a half-life of  $\sim 2.6$  years, decays through the  $\beta^+$  process shown above to an excited state of Neon-22, which then undergoes another decay through  $\gamma$ -emission, emitting a photon of  $1.275\text{MeV}$ . Another subsequent pair of photons are emitted after the positron from  $\beta^+$  decay annihilates with an electron, with energies of  $0.511\text{MeV}$ . The decay scheme can be viewed below:

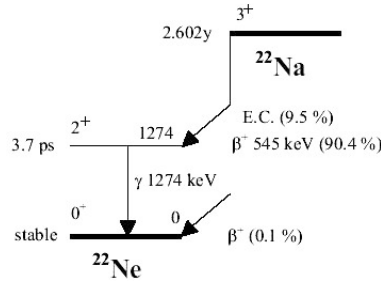


Figure 4: Decay Scheme for Na-22. [3]

## 2.2 Scintillators

This lab made use of two types of scintillators: plastic and Sodium-Iodide, each serving different purposes. A plastic scintillator refers to a scintillator in which the fluor, the primary fluorescent emitter, is suspended in a solid polymer base. A plastic scintillator is advantageous in that there is a high light output and a relatively quick signal, with a decay time from about 2-4ns. They are mostly used for their ability to be shaped into any desired form, as well as their durability.

The sodium-iodide ( $\text{NaI}$ ) scintillator used in lab is an example of an inorganic scintillator, which consist of crystals grown in high temperature furnaces. Our  $\text{NaI}$  scintillator is also doped with thallium and produces a blue scintillation light. However, these types of scintillators have a disadvantage in that they are hygroscopic, an ability to absorb moisture from the air. This requires that they be encased in an airtight container to prevent any moisture from seeping in. Yet despite these limitations, the inorganic crystals are able to be cut into small individual pieces and arranged in arrays to provide position sensitivity, giving them an advantage over plastic scintillators.

### 3 Apparatus

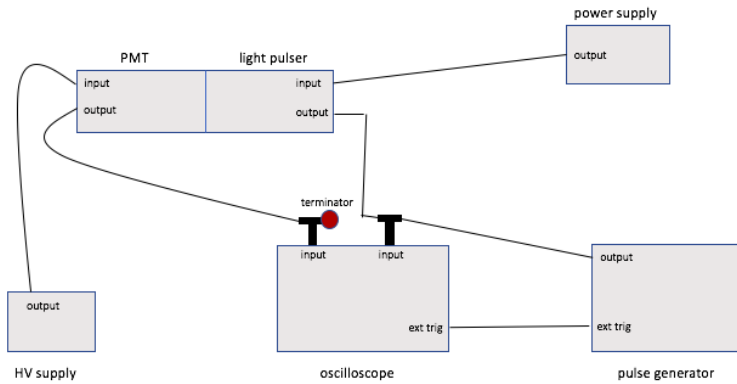


Figure 5: First apparatus used in "Photomultiplier Response." Contains a BNC 8010 NIM pulse generator,  $50\Omega$  terminator, 10 stage Electron Tubes 9266KB PMT, light pulser, Standford Model P325 high voltage supply, and Harrison 6289A power supply.

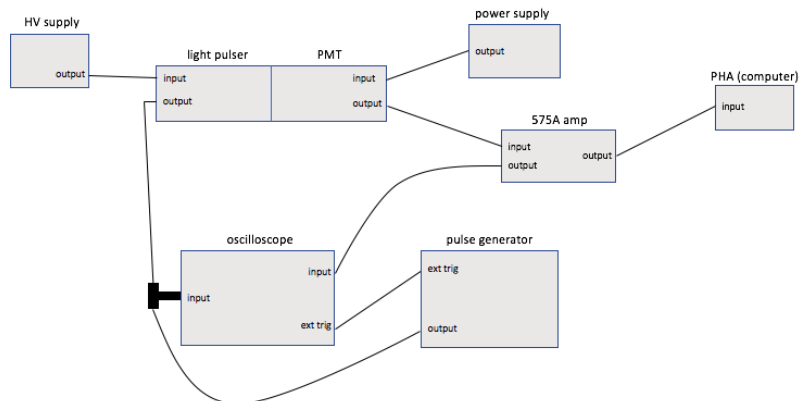


Figure 6: Second apparatus used in "Photomultiplier Response." Addition of an Ortec 575A Pulse-Shaping Amplifier, as well as a Pulse Height Analyzer(PHA) on the computer.

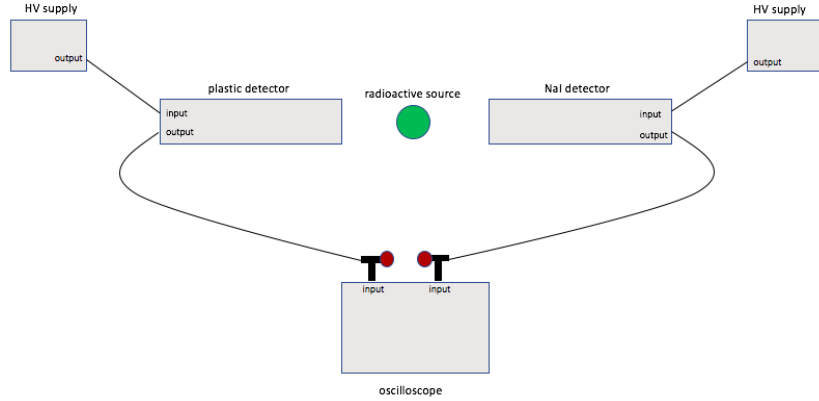


Figure 7: Apparatus used for "Comparison of Plastic and NaI." Addition of the second PMT (NaI) and respective power supply.

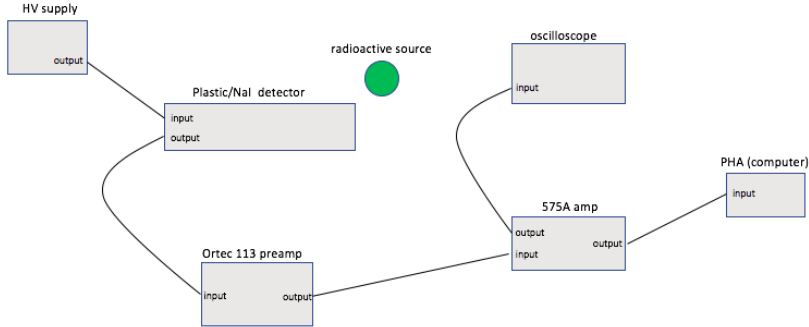


Figure 8: Apparatus used for "Pulse Height Spectra", same to prior apparatus, rearranged for pulse height measurements.

## 4 Procedure

### 4.1 Photomultiplier Response

In this section, we are essentially simulating the light output of a scintillator using a light pulser to explore the gain of a photomultiplier tube (PMT).

To do so, we must first make the pulser give appropriate light pulses. We connect the trigger output of a square pulse generator to the external trigger on the oscilloscope, as well as the generator output to the channel 1 input, terminated with  $50\Omega$ . Next, the pulser was configured by varying the pulse width and power supply voltage, to remove saturation. Once we were able to see a light pulse from the LED, we inserted the phototube into the pulser housing, taping the end of the housing to prevent any light leakage. This apparatus can be viewed in Figure 5. Then the signal characteristic (width, peak, etc.) were noted while varying the DC Voltage, pulse width, and pulse height, the data for which can be viewed in the data section. After these variations, we performed further variations of input voltages to determine how the PMT responds with different voltages.

The next step was to include the Pulse Height Analyzer(PHA) to aid in studying PMT fluctuations. The Ortec 575A Pulse-Shaping Amplifier was added to the apparatus, shown in Figure 6. The output of the amplifier was made to create a pulse with amplitude +5V. This NIM module was used to amplify and shape the input signal such that it can be interpreted by the PHA software on the computer.

## 4.2 Plastic vs NaI Scintillators

This section added in another Scintillation counter, to create the apparatus shown in Figure 7. A Cs-137 source was placed equidistant from both detectors, and data collected from both. We saw that the time response for the NaI detector was significantly slower than that of the plastic detector.

## 4.3 Pulse Height Spectra

Finally, the pre-amp, amplifier, and computer were added into to the circuit, displayed in Figure 8. This apparatus was used for further comparison between the NaI and plastic detectors, as well as collecting spectrum data for several radioactive sources, mentioned in sections 2.1.1 - 2.1.4

# 5 Data

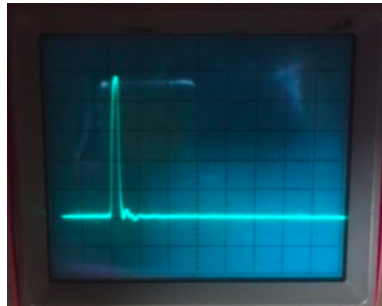


Figure 9: Pulse generated in "PM response." (scale:  $0.05\mu\text{s}/\text{cm}$  vs  $1\text{V}/\text{cm}$ )

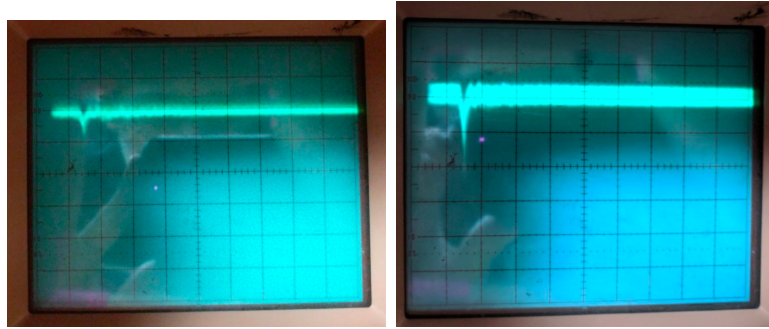


Figure 10: Left: Noise from PMT using 800V. Right: Noise from PMT using 900V. (scale: 0.05 $\mu$ s/cm vs 2mV/cm)

Table 1: Data from "PM Response" varying Pulse Width, DC Voltage, and Pulse Height.

| INPUT       |                |                  | OUTPUT       |                     |               |                      |
|-------------|----------------|------------------|--------------|---------------------|---------------|----------------------|
| pulse width | DC voltage (V) | pulse height (V) | signal width | uncertainty (width) | signal height | uncertainty (height) |
| 0.03us      | 25             | 3                | 0.2us        | 0.15us              | 150mV         | 25mV                 |
| 0.03us      | 28             | 3                | 0.2us        | 0.15us              | 150mV         | 25mV                 |
| 0.03us      | 32             | 3                | 0.2us        | 0.15us              | 170mV         | 25mV                 |
| 0.03us      | 36             | 3                | 0.2us        | 0.15us              | 200mV         | 25mV                 |
| 0.03us      | 40             | 3                | 0.2us        | 0.04us              | 400mV         | 50mV                 |
| 30ns        | 30             | 3                | 0.2us        | 0.1us               | 150mV         | 50mV                 |
| 35ns        | 30             | 3                | 0.2us        | 0.05us              | 350mV         | 40mV                 |
| 40ns        | 30             | 3                | 0.25us       | 0.025us             | 500mV         | 50mV                 |
| 45ns        | 30             | 3                | 0.25us       | 0.025us             | 850mV         | 50mV                 |
| 50ns        | 30             | 3                | 0.35us       | 0.0125us            | 1.05V         | 50mV                 |
| 50ns        | 30             | 3.2              | 0.35us       | 0.0125us            | 1.05V         | 50mV                 |
| 50ns        | 30             | 3.4              | 0.38us       | 0.02us              | 1.04V         | 20mV                 |
| 50ns        | 30             | 3.6              | 0.38us       | 0.02us              | 1.04V         | 20mV                 |
| 50ns        | 30             | 3.8              | 0.35us       | 0.02us              | 1.04V         | 20mV                 |
| 50ns        | 30             | 4                | 0.37us       | 0.02us              | 1.04V         | 20mV                 |

Table 2: Data from "PM Response" varying high voltage input.

| INPUT       |                |                  | OUTPUT           |              |                     |               |                      |
|-------------|----------------|------------------|------------------|--------------|---------------------|---------------|----------------------|
| pulse width | DC voltage (V) | pulse height (V) | high voltage (V) | signal width | uncertainty (width) | signal height | uncertainty (height) |
| 0.03us      | 20             | 3                | 400              | 0.025us      | 0.025us             | 0.4mV         | 0.4mV                |
| 0.03us      | 20             | 3                | 600              | 0.175us      | 0.025us             | 5mV           | 1mV                  |
| 0.03us      | 20             | 3                | 900              | 0.175us      | 0.025us             | 125mV         | 25mV                 |

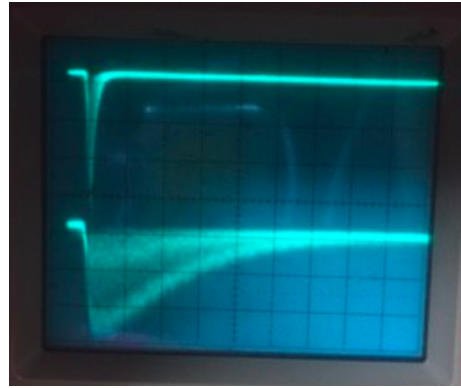


Figure 11: Comparing Cs-137 signals from plastic(top) and NaI (bottom) detectors.

## 6 Analysis

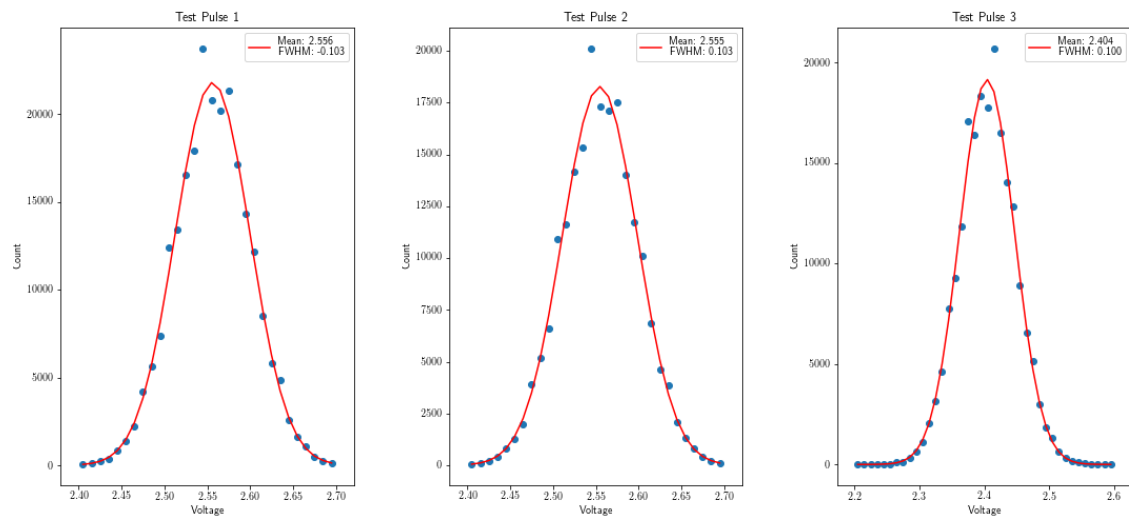


Figure 12: Test Pulses with Gaussian Fits and FWHM from "PM Response"

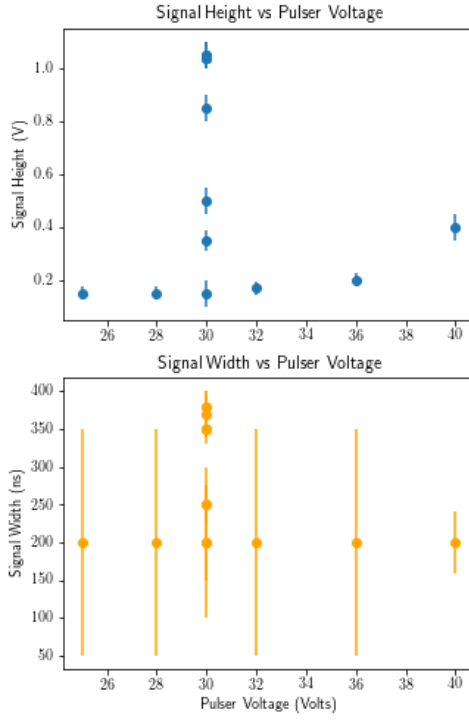


Figure 13: Effects of varying Pulse voltage on the output signals width and height.

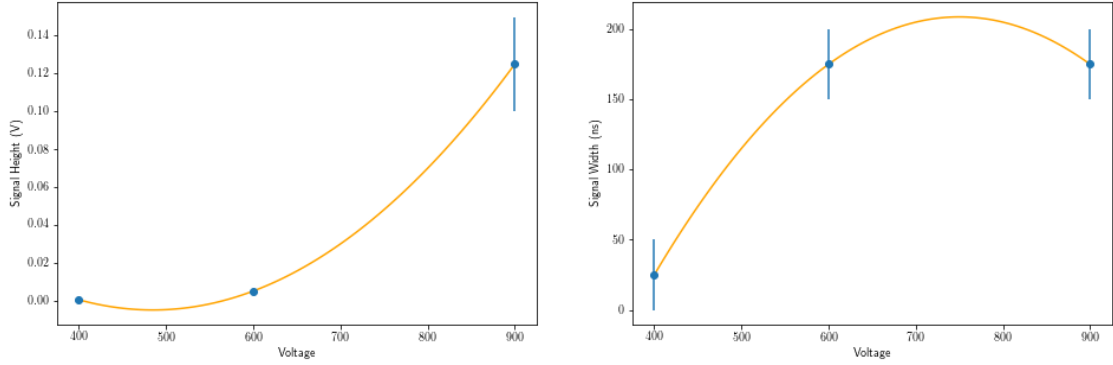


Figure 14: Effects of varying High voltage on the output signals width and height.

Looking at Figure 13, we can see that with an increase in DC voltage to the pulser, we see a slow, eventually rapid increase in signal height at around 36-40V. There are a few things to point out about Figure 13: The spike at 30 Volts in both graphs coincides with other effects responsible for the increase. For the top graph, the spike can be attributed to an increase in pulse width, while for the bottom graph, the spike coincides with an increase

in pulse height. Therefore, it is very apparent that these two values are very closely related in producing the shape of the output pulse.

As for uncertainties, we can see that the uncertainty in Signal Height remained relatively constant. However, there are more interesting features when looking at the uncertainty in Signal Width. For instance, we may have started to see a trend such that an increase in pulser voltage creates a decrease in signal width uncertainty, however, this is only shown by a decrease in uncertainty for the rightmost point. As for the spike at 30 Volts, we definitely see an decrease in uncertainty due to changes in pulse width and pulse height.

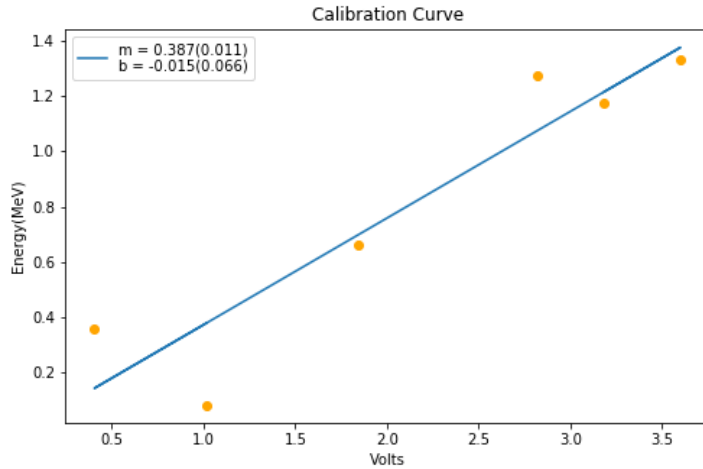


Figure 15: Calibration Curve fit to photopeaks and their known energies. The uncertainty in fit-parameters are shown adjacent in parenthesis.

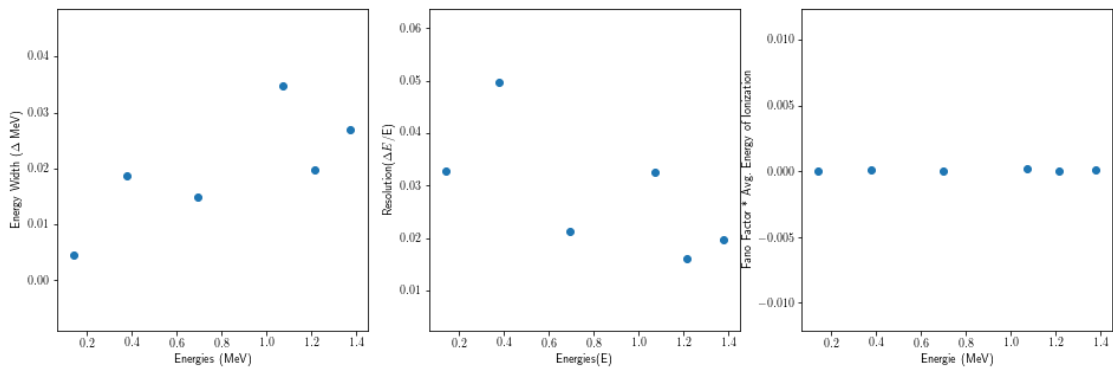


Figure 16: (Extra Credit) Uncertainties, Resolution, and Fano Factor\*Avg. Energy of Ionization, respectively. We get FW  $\approx 0$

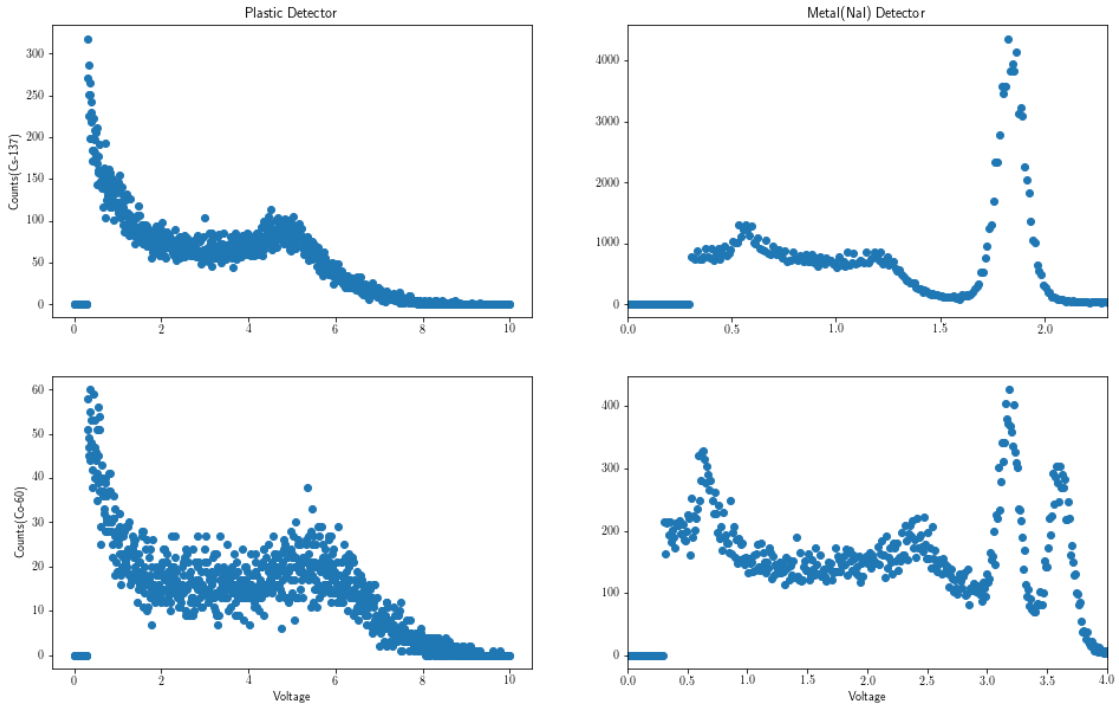


Figure 17: Comparing the spectra of Cs-137(top) and Co-60(bottom) between plastic(left) and metal(right) detectors

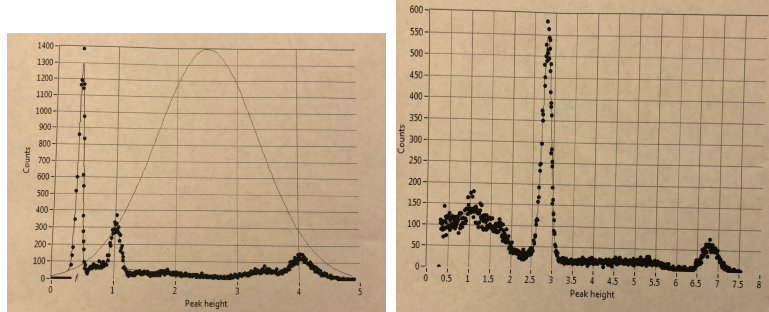


Figure 18: Spectra with Gaussian Fits for Ba-133(left) and Na-22(right).

## 7 Results

All of our obtained results can be viewed in the above sections (Data and Analysis), along with their quoted uncertainties. However, there is some incomplete data that we were unable to obtain. Ideally, we would have collected more data points to add in Table 2, when testing the effect of varying high voltage input. Unfortunately, we spent too much time acquiring the

preceding data set, as well as creating a working apparatus, to comprehensively determine such effects. The highest order function we are able to fit to the data from Table2 is only that of a parabola, when in actuality, we know their respective shapes to be more intricate, consisting of exponentials and areas of constant saturation.

As for the comparison between metal and plastic detectors, Figure 17 shows how much detail is lost when using a plastic detector. We do not see any of the photopeaks of interest when using a plastic detector, and we can therefore conclude that a metal (NaI) should be used over a plastic detector. A source of error in this analysis could be from our calibration of the gain. This is further confirmed in that both spectra for the plastic detector look approximately the same. We also see a difference in the number of counts for the radioactive source. This could potentially be due to the different response times and decay times for each detector, as shown in Figure 11.

And finally, as for the spectra obtained, we were able to take spectra for all four radioactive sources, as well as fit Gaussian distributions to them in order to find peak heights and their corresponding energies. We used the state probabilities and compared the counts for each peak, as well as the relative energies to determine which peak was associated with their respective energy. In doing so, we were able to make our calibration curve. For Co-60, we found the peak at 3.2V to coincide with 1.17 MeV, and 1.33MeV for the peak found at 3.6V. As for Cs-137, we assigned the peak at 1.82V with the photon energy 0.66MeV. The spectra for Ba-133 and Na-22 went through the same process of assignment. In Ba-133, we assigned the first two prominent peaks to be 383KeV and 437KeV, respectively, and in Na-22, we assigned the first peak to the 0.511MeV photon energy and the second smaller peak to the 1.275 MeV photon energy. These data points can all be viewed in the Calibration Curve in Figure 15. The sources of these photons and their respective energies are discussed in §2.1.

## 8 Discussion

Despite having smaller data sets, we were still able to complete all the sections in this lab. In doing so, we were adequately able to compare the abilities of a NaI detector versus a plastic detector, as well as characterize the response of a photomultiplier, leading up to our final spectrum data for all four radioactive sources. This lab was an overall success, in that we reached all of our goals, learned what to and what not do to for further labs, and did it all while safely handling radioactive sources and high voltage instruments.

## References

- [1] Ervin B. Podgoršak. *Modes of Radioactive Decay*, pages 475–521. Springer Berlin Heidelberg, Berlin, Heidelberg, 2010.
- [2] Jaeger H. University of Miami. Ba-133 decay scheme.
- [3] Iva Bartošová, V Slugeň, J Veterníkova, Stanislav Sojak, Martin Petriska, and Amine Bouhaddane. Non-destructive research methods applied on materials for the new generation of nuclear reactors. 516:012023, 06 2014.